npj Computational Materials

www.nature.com/npjcompumats

ARTICLE OPEN

Check for updates

Reactive pathways toward parasitic release of singlet oxygen in metal-air batteries

Adriano Pierini[1], Sergio Brutti[1,2] and Enrico Bodo[1]✉

The superoxide disproportionation reaction is a key step in the chemistry of aprotic metal oxygen batteries that controls the peroxide formation upon discharge and opens the way for singlet oxygen release. Here we clarify the energy landscape of the disproportionation of superoxide in aprotic media catalyzed by group 1A cations. Our analysis is based on ab initio multireference computational methods and unveils the competition between the expected reactive path leading to peroxide and an unexpected reaction channel that involves the reduction of the alkaline ion. Both channels lead to the release of triplet and singlet O_2. The existence of this reduction channel not only facilitates singlet oxygen release but leads to a reactive neutral solvated species that can onset parasitic chemistries due to their well-known reducing properties. Overall, we show that the application of moderate overpotentials makes both these channels accessible in aprotic batteries.

npj Computational Materials (2021)7:126 ; https://doi.org/10.1038/s41524-021-00597-3

INTRODUCTION

Incumbent societal challenges as the electrification of mass-transportation or aviation require a rush beyond the state-of-the-art in the way energy is stored and released[1,2]. This transition imposes a leap in battery performance and safety without jeopardizing the recent efforts for providing environmental-friendly technologies[3,4]. Since the last decades of the XX century, and pushed by an extraordinary collective effort, battery science is experiencing an astounding era of exploration through which an unprecedented variety of electrochemical systems has been proposed and studied in the last years[5–12]. The future success of novel battery paradigms roots in these fundamental studies, that are paving the way for technological breakthroughs and novel energy storage devices.

Aprotic metal-air batteries have theoretical figures that are one order of magnitude larger than those based on Li-ion/Na-ion paradigms[13–17]. However, all Li–O_2, Na–O_2, K–O_2, Mg–O_2, and Ca–O_2 systems are still in their infancy, being their respective fundamental electrochemistry still under debate under many aspects.

Parasitic chemistries at positive electrodes in all metal-O_2 batteries are the foremost obstacle that hinders the reversible operation of the redox system and thus of the entire battery. The current understanding of all alkaline-Me-O_2 systems (Me = Li, Na, K) suggests a common pattern in the degradation mechanism, originating from (a) the nucleophilic attacks of reduced reactive oxygen species, i.e., MeO_2, O_2^-, MeO_2^-, O_2^{2-} [18–22] (b) the formation of hydrogen peroxide starting from protons or water molecules[23,24], or (c) the high reactivity of singlet oxygen molecules[25] generated either by oxidation of peroxides[26–28] or chemical disproportion of superoxide species mediated by weak Lewis acids[24,26,29,30]. Overall, the experimental evidence of singlet oxygen release in all alkaline metal-O_2 systems[24] poses serious fundamental questions concerning the thermodynamics and kinetics of these reactions. Apparently, the reactive mechanism that drives/hinders the singlet oxygen release is only drafted and poorly rationalized for alkaline metals beyond lithium.

Here we tackle the challenge to analyze the thermodynamics of the competitive disproportionation reaction channels of sodium and potassium superoxide in close comparison with LiO_2, using multireference ab initio methods. The aim of this work is to shed light on the fundamental thermodynamics of two competitive paths that are involved in the onset of parasitic chemistries in metal-air batteries.

RESULTS AND DISCUSSION

The superoxide disproportionation reaction

$$O_2^- + O_2^- \rightarrow O_2^{2-} + O_2 \quad (1)$$

is a key ingredient of the chemistry of metal-air batteries. As it is widely known, and as we have shown in a previous paper[23] this reaction evolves toward two possible products depending on the multiplicity of the resulting neutral oxygen molecule.

Reaction (1) is highly unlikely to take place in its pure anionic form without a cation, because the two superoxides repel each other via Coulomb forces. The presence of positive ions such as H^+, Li^+, Na^+, and K^+ weakens the Coulomb repulsion and allows the reaction to proceed. The most effective ion in catalyzing the reaction is the proton which makes it exothermic[7], while the alkali metals are less efficient, and their reaction profiles are endothermic. In a set of previous calculations[23], we have unequivocally shown that the reaction is dominated by thermodynamics and that kinetic plays only a limited role. The scheme of reaction (1) in the presence of metal is shown in Fig. 1.

The MO_4^- superoxide complex on the left of Fig. 1a is made by two superoxide anions that, each being a doublet, can arrange themselves in a singlet or triplet state. In the reactants channel, the two multiplicities have very similar energies. The system evolves toward the right forming a peroxide MO_2^- plus an O_2 neutral molecule either in its $^3\Sigma$ or $^1\Delta$ states. In the product region, the energy difference between the singlet and the triplet state is significant and about 1 eV. The detailed path of the reaction has been explored using correlated multiconfigurational methods by

[1]Department of Chemistry, University of Rome "La Sapienza", Rome, Italy. [2]GISEL—Centro di Riferimento Nazionale per i Sistemi di Accumulo Elettrochimico di Energia, Firenze, Italy. ✉email: enrico.bodo@uniroma1.it

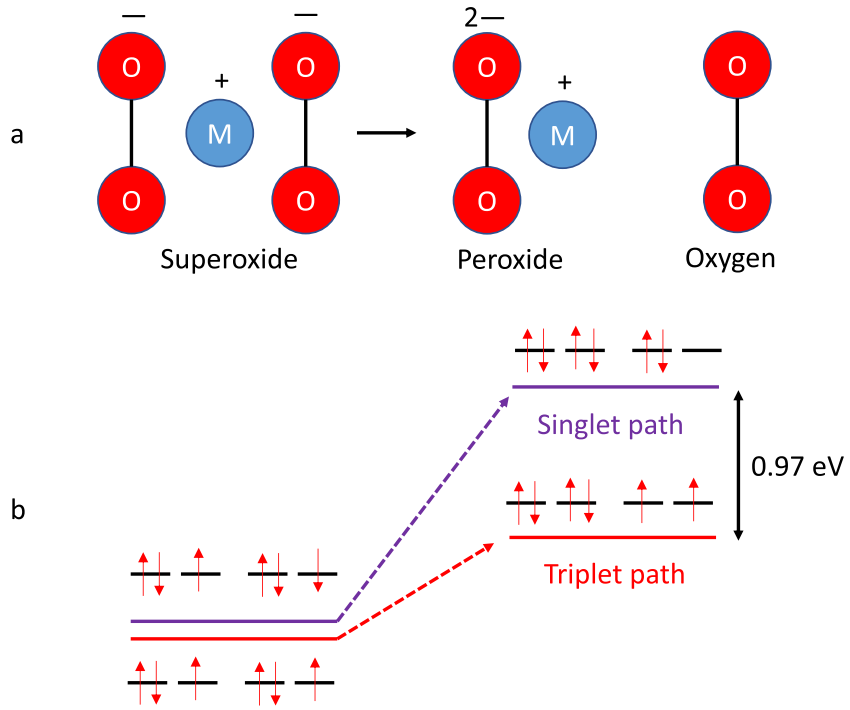

Fig. 1 Scheme of reaction (1). a The MO_4^- superoxide complex evolves into a peroxide MO_2^- and a neutral oxygen molecule. **b** The typical energetic profile is endoergic and the simplified electron arrangements in the [O—O] π orbitals are shown.

us in ref. [23] for the H^+ and Li^+ ions. The former has an exoergic path, the latter an endothermic one. In other words, it turned out that, in the absence of protons, the reaction leading to singlet oxygen in the Li^+ catalyzed reaction requires energy and is not spontaneous.

While our calculations clearly pointed in favor of a strong catalytic action of protons, the role of H^+ (and ultimately that of water) in the disproportion (1) is still poorly understood and contrasting evidence has arisen in time[27,31,32] as recently summarized by Hong and Byon[33]. While the role played by proton sources such as water is still controversial, the larger amounts of singlet oxygen arising in Na–O_2 cells is a somewhat surprising result since reaction (1) with Na^+ is expected to be more endothermic than that with Li^+.

The difficulties in explaining the amount of singlet oxygen release by reconciling what is seen by experiments and the calculated reaction paths clearly points to the fact that the mechanisms of reaction (1) may not be quite as straightforward as initially thought.

In our opinion, the subtleties in the mechanism, are due to the intrinsic multiconfigurational nature of the electronic configurations involved. Single reference approaches (including DFT or MP2) naturally fails to correctly evaluate the simultaneous presence of more than one determinant (that roughly corresponds to a single Lewis structure) and to correctly account for the possible existence of multiple schemes of electronic occupations. The issue does not simply reduce to the presence of different multiplicities, but rather to the possibility of overlooking certain electronic configurations which might exist at a given geometry of the nuclei.

For this reason, we have carried out tailored calculations using a multiconfigurational space which should be large enough to include all the possible electronic occupation schemes of the metal and oxide moieties. This space stems from the *p* orbitals of the oxygen atoms that are responsible for the electronic rearrangements (see Fig. 1), and the valence *s* orbital on the metal. This multiconfigurational approach in treating reaction (1) should ensure that all possible low-lying energetic configurations, hence all possible reactive channels are included, even those that defy obvious chemical expectations.

To keep the presentation simple, and following our previous results[23], we have decided to analyze reaction (1) exclusively from the point of view of thermodynamic. First of all, the initial formation of the superoxide complex MO_4^- is an exothermic reaction with no kinetic barrier. Therefore, we consider the superoxide complex as the initial reference point of our investigation. We remark that the triplet-singlet energy gap in MO_4^- is negligible and irrelevant for the following discussion. Secondly, we know from our previous calculations that the evolution of the complex toward the peroxide follows a path where the kinetic barriers are lower than or substantially equal to the final energies of the products, hence they can hardly be the source of any relevant obstacle to reaction beyond thermodynamics.

For these reasons, to sample the thermodynamic of reaction (1), we can limit ourselves to consider the following dissociation process:

$$MO_4^- \rightarrow MO_2^- + O_2 \quad (2)$$

The energies of the three species have been evaluated separately using the correlated multiconfiguration approach mentioned above and suitable MP2 geometries (see Methods section). The energy variation along reaction (2) has been simply obtained as

$$\Delta E = E(O_2) + E(MO_2^-) - E(MO_4^-) \quad (3)$$

where the energies involved depend on the multiplicity of O_2 and on the electronic state of MO_2^-.

The geometries of the LiO_4^- and LiO_2^- species at the MP2 level with the relevant geometric information are shown in Fig. 2. The respective ones for Na^+ and K^+ are displayed in Supplementary Figs. 1 and 2. The LiO_4^- complex has a symmetric shape with the two superoxides $[O—O]^-$ groups bound to the central ion and oriented at 90° with respect to each other. The M—O distances in MO_4^- increases as the ionic radius of the alkali increases, moving from 1.89 Å for Li^+ to 2.25 Å for Na^+ and 2.62 Å for K^+. The [O—

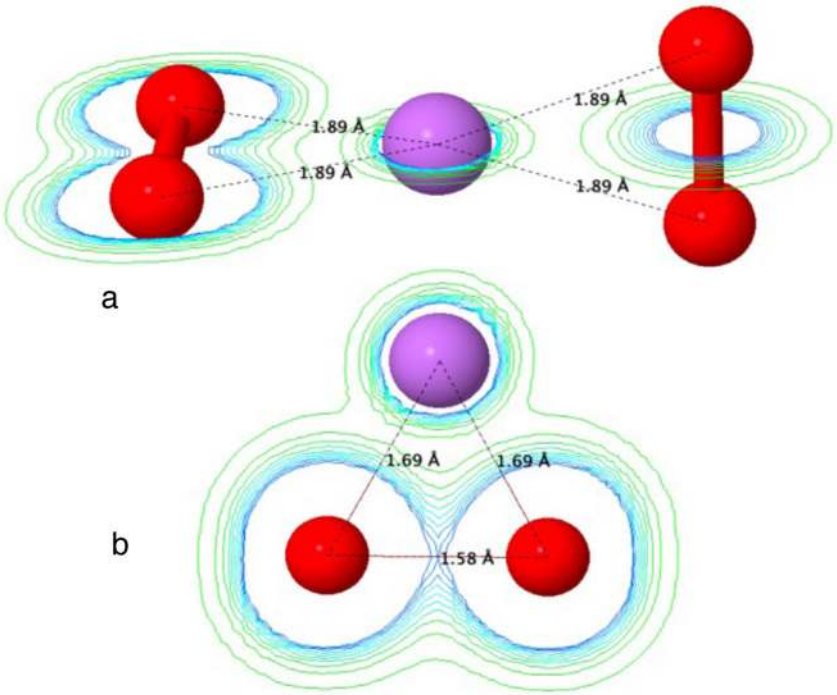

Fig. 2 Geometries of the Li superoxide and peroxide complexes. a The LiO_4^- superoxide complex. **b** The LiO_2^- peroxide complex. The M—O distances are reported to highlight the symmetry. The CASSCF(18,13) electronic density is reported on the *xy* plane as contours.

Table 1. NEVPT2 energies (in eV) of the transformation of MO_4^- in peroxide $MO_2^- + O_2$. The values refer to ground state $O_2(^3\Sigma)$. The values in parenthesis pertains to $O_2(^1\Delta)$. Approximate values for H^+ have also been reported for comparison.

Ion	Vacuo	Diethyl ether	Acetonitrile
Li^+	3.28 (4.25)	2.33 (3.29)	1.92 (2.88)
Na^+	3.85 (4.1)	2.67 (3.63)	2.15 (3.11)
K^+	3.82 (4.78)	2.61 (3.57)	2.10 (3.06)
H^+ [a]	1.01 (1.97)	−0.28 (0.68)	−0.49 (0.47)

[a]Triplet energies for H^+ have been obtained with DFT and the B2GP-PLYP[57] functional, the energies of the singlet channels have been estimated by summing the NEVPT2 singlet-triplet splitting in isolated O_2.

$O]^-$ distance is constant at 1.35 Å. The MO_2^- peroxide is a triangle with the $[O—O]^{2-}$ distance varying only slightly with the accompanying ion from 1.57 to 1.59 Å. The M—O distances are 1.69 Å for Li^+, 2.06 Å for Na^+, and 2.34 Å for K^+.

The path to the peroxide

As shown in detail in ref. [23], the path to the peroxide formation is straightforward and follows closely the scheme in Fig. 1. The metal retains its positive charge all along the dissociation reaction (2) which is driven by the transfer of the π unpaired electron of one of the superoxide doublets into the hole of the π orbital of the other. This electron transfer produces a closed shell peroxide ion and a neutral oxygen molecule. Along this reaction path, the [O—O] distance is 1.35 Å in MO_4^- and becomes 1.6 Å in the MO_2^- product. The latter value is the key to recognize the formation of a peroxide. The energies involved in the transformation (2) for the formation of the superoxide depend on the multiplicity of the neutral O_2 molecule. They are reported in Table 1.

All reactions involving an alkali metal are endothermic and require a substantial amount of energy for singlet oxygen formation (4.1–4.8 eV in vacuo). The trend for reaction energies in the gas phase is $H^+ \ll Li^+ < Na^+ \sim K^+$.

The inclusion of a solvent (albeit in an approximate fashion through the SMD model) alters this trend only slightly. The general effect of the solvent is that of stabilization of the $MO_2^- + O_2$ products due to the presence of two solvation shells, hence greater solvation energy with respect to the single molecular complex MO_4^-. The stabilization is greater for the solvent with a larger dielectric constant (acetonitrile), but, despite this, the reaction leading to singlet oxygen remains endothermic at about 2.9–3.5 eV for all metals.

The path to a reduced metal superoxide

The triangular structure reported in Fig. 2b is a peroxide with the $[O—O]^{2-}$ distance around 1.6 Å. The electronic multiplicity is a singlet, and the valence electrons are essentially occupying the π orbitals of the peroxide ion. The *s* orbital on the metal is empty. However, we have found that another electronic state of this complex exists and that its energy can be lower than the peroxide depending on the value of the O—O distance. We noticed that, if this distance is reduced to around 1.35 Å, i.e., the typical distance of a superoxide ion, the lowest energy electronic configuration corresponds to an electron in the *s* orbital of the metal and to the [O—O] moiety in a doublet state with a partially occupied π shell. In other words, there are geometries on the potential energy surface where the reduction of the metal (by oxidation of one of the superoxide ions) becomes accessible and less energetic than the disproportionation of the two superoxides. This process, whose likelihood depends on the O—O distance leads to the generation of a $M^0O_2^-$ complex. The latter is essentially a global singlet state made of two doublets with unpaired electrons occupying the π orbital of the $[O—O]^-$ superoxide and the *s* orbital on the metal. An updated version of the scheme of Fig. 2, now including both the peroxide and the superoxide is shown in Fig. 3.

The optimal geometries of the reduced metal complexes $M^0O_2^-$ are difficult to obtain using single reference methods (this is probably the reason why they did not appear in the literature

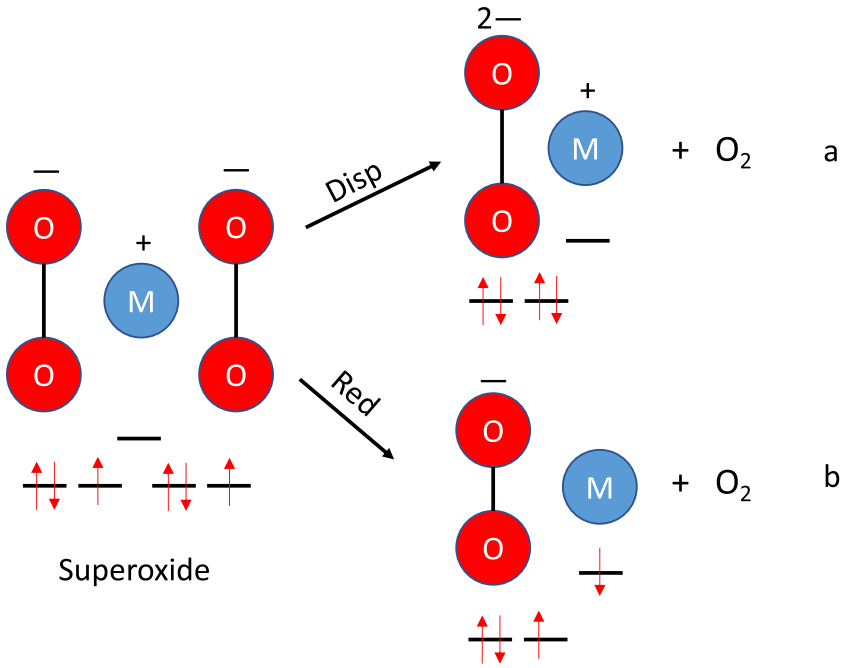

Fig. 3 Scheme of reaction (1) in the triplet state including the metal reduction channel. The MO_4^- superoxide complex evolves into: **a** A peroxide MO_2^- and a neutral triplet oxygen molecule (the same as in Fig. 1). **b** An $M^0O_2^-$ complex through a reduction of the metal. The simplified electron arrangements in the involved π and *s* orbitals are shown.

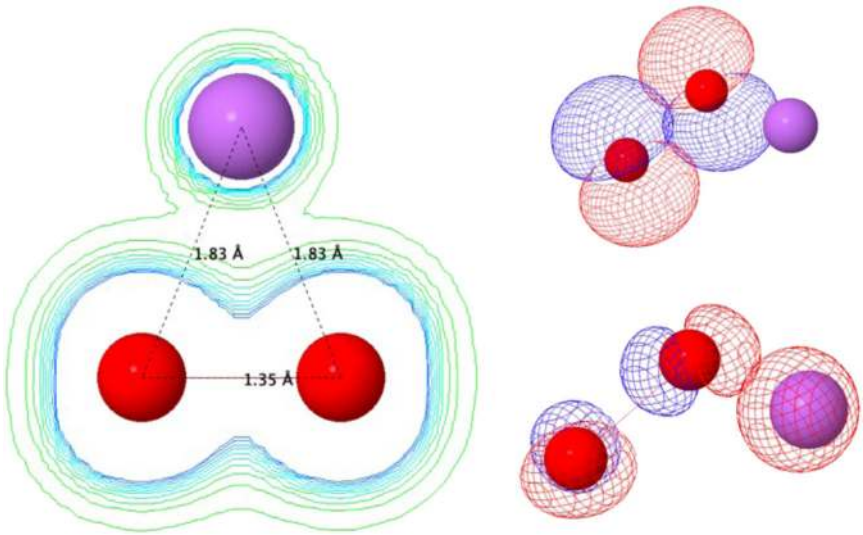

Fig. 4 Minimum geometry and orbitals of the superoxide complex $Li^0O_2^-$. The M—O distances are reported to highlight the symmetry. The CASSCF electronic density is reported on the molecular plane as contours. The two singly CASSCF occupied orbitals are also reported.

before). In order to make the SCF procedure converge to them it is necessary to use a broken symmetry approach whereby the unrestricted orbitals are forced to be asymmetric. When this is done the resulting geometries retain the typical [O—O] distance of the superoxide and the metal acquires an electron. The geometry of the $Li^0O_2^-$ is reported in Fig. 4 along with the two half-filled CASSCF orbitals.

The metal reduction channel leading to $M^0O_2^-$ appears, from our calculations, to compete in energy with the disproportion leading to the peroxide. The relevant energy values are reported in Table 2.

Table 2. NEVPT2 energies (in eV) of the transformation of MO_4^- into $M^0O_2^- + O_2$. The values refer to ground state $O_2(^3\Sigma)$. The values in parenthesis pertains to $O_2(^1\Delta)$.

Ion	Vacuo	Diethyl ether	Acetonitrile
Li^+	2.61 (3.57)	2.97 (3.93)	3.06 (4.02)
Na^+	2.11 (3.07)	2.42 (3.38)	2.52 (3.48)
K^+	1.81 (2.77)	2.25 (3.21)	2.38 (3.34)

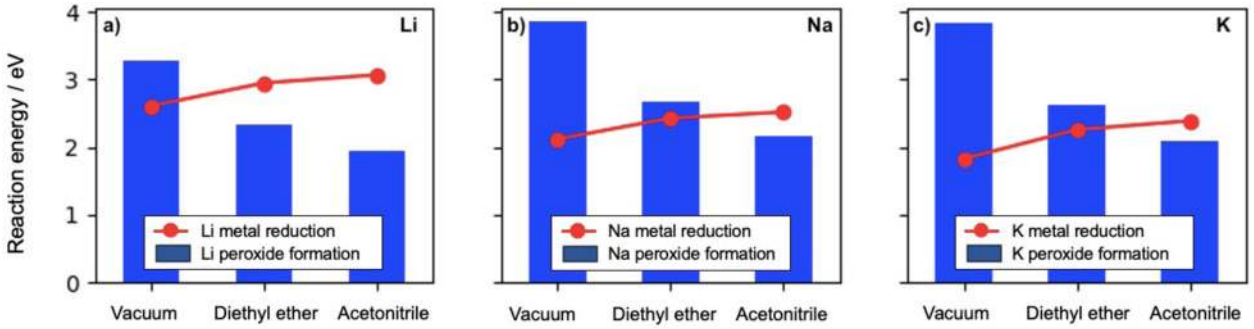

Fig. 5 Superoxide reduction vs metal reduction. Energies of the peroxide channel (blue bars) vs energies of the metal reduction channel (red circles) with respect to the MO_4^- complex: **a** Li, **b** Na and **c** K.

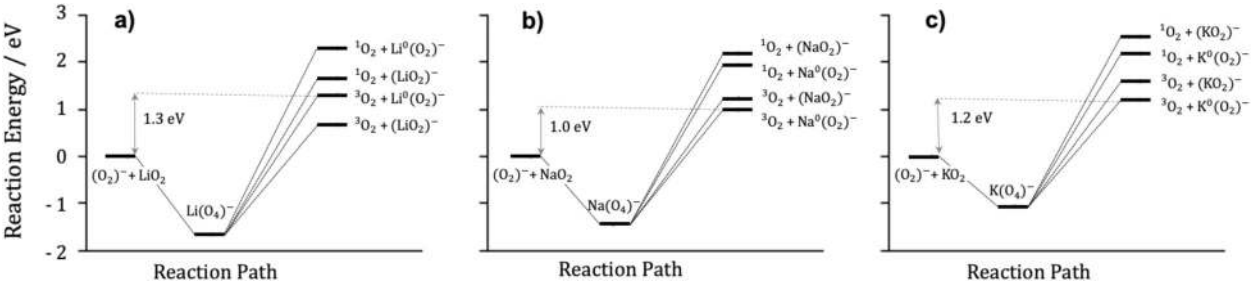

Fig. 6 Disproportionation/reduction reaction thermodynamics. Competitive reaction paths for **a** Li, **b** Na, and **c** K superoxide dimers calculated in diethyl ether. The number in eV indicates the energetic barriers to the first available channel that leads to ODR (i.e., singlet oxygen or neutral metal see text for details).

When in vacuo, the reaction leading to triplet oxygen appears at values ranging from 2.6 to 1.8 eV with a trend that is $Li^+ > Na^+ > K^+$ which is opposite to the one found for the peroxide channel. In other words, when moving from Li^+ to K^+ the metal reduction channel is more and more energetically favored while the superoxide formation is less and less likely.

The reduction channel leading to $M^0O_2^-$, contrarily to the disproportion one is not favored by the presence of a solvent, but instead its energy increases when increasing the polarity and dielectric constant of the medium. This can be understood by considering that the $M^0O_2^-$ complex has a small charge separation and, hence its solvation energy decreases with solvent dielectric constant.

A pictorial way to represent the situation is reported in Fig. 5, where we report the energies of the disproportionation to the peroxide (blue bars) vs the energies of the metal reduction channel (red circles), both for the formation of the triplet oxygen.

The energies required to form singlet oxygen are larger than ~1 eV in both channels. For each ion we show the results in vacuo and in the two solvents. We stress that the results in the solvent are only approximate since the solvent in the calculation is rendered as a continuum with a molecule-containing cavity. The real solvent might produce additional effects due to the presence of real molecules which are not accounted for in these calculations.

We clearly see that the reduction channel is always competitive with the disproportionation and that the energies required to form singlet or triplet oxygen, if available, would necessarily also open the reduction process at the expense of the metal ion.

For Li^+ (panel **a** of Fig. 5), the reduction channel is the preferred reaction pathway in vacuo (by ~0.5 eV), while it is destabilized (by ~1 eV) in the presence of a solvent. The likelihood of reducing the metal (in solution) is very low for this ion. Hence, the production of singlet oxygen must come from the disproportionation channel that requires 2.9–3.3 eV depending on the solvent polarity (Table 1, first row).

Moving to Na^+, the reduction of the metal is by far the most likely process in vacuo since it turns out to lie ~1.7 eV below the peroxide one. When moving to diethyl ether which has a low dielectric constant the reduction is at par with the disproportionation while its energy is slightly above the latter when the dielectric constant increases (acetonitrile). It is remarkable that, if we take the energy values in vacuo for Na^+, then the threshold to produce singlet oxygen by metal reduction lowers to only 3 eV instead of the 4.8 eV needed if the reaction followed the peroxide formation path. A similar huge energy gain can be seen for K^+ where the reaction involving the metal reduction needs 2 eV less than the disproportionation to peroxide.

Our computational model has been kept purposedly simple to allow for the tracing of the correct electronic state of each molecule involved in the reaction mechanisms. Nevertheless, it is possible to explore the effect due to the additional presence of a second metal cation that binds the O_2^- reagent and the MO_2^- product. This has been done and the results are presented in the Supplementary Discussion and in Supplementary Table 3.

Impact on Li–O_2, Na–O_2, and K–O_2 battery operation

The competition between the disproportionation and the metal reduction channels starting from the superoxide dimers unavoidably alters the consolidated reaction landscape in aprotic Li-, Na- and K-O_2 batteries. In Fig. 6 we summarize the potential energy surfaces of the formation and evolution of the negatively charged lithium, sodium, and potassium superoxide dimers in the model solvent for diethyl-ether. There we highlighted the energy required to give the most stable products able to initiate a degradation/parasitic chemistry in batteries (onset degradation reactant, ODR) either it being singlet oxygen or neutral alkali metals. Neutral metal atoms can act as ODR or as agents promoting a parasitic chemistry because of their well-known reducing properties and of their propensity to attack protic impurities and oxygen molecules.

The reaction paths start from the bimolecular dimerization (which is exoergic) and proceeds by dissociating into a metal complex and a free oxygen molecule. The latter step is highly endoergic and, in this respect, one may safely assume that it represents an insurmountable energetic barrier at room temperature. Remarkably, for Na and K metal ions, the lowest-lying dissociation channel is an ODR one leading to the reduction of the metal atom. Overall, the energies required to activate ODR paths are larger than 1 eV, and therefore none of these reactive channels are active in equilibrium conditions at room temperature[34].

In all batteries, overpotentials are required to allow ionic transport in the electrolyte (ohmic drop) and to overcome the activation energy (electron transfer overpotential) at the electrode/electrolyte interphase to initiate any redox reaction[35,36]. Electron transfer phenomena in electrochemical systems have been scouted by Markus and collaborators in many landmarking papers[35,37–42]. Under the assumption of a direct energy transfer from the polarization overpotential to the internal energy of redox reagents[35,39], the application of large overpotentials can provide the superoxide species enough kinetic energy to climb the activation energies for disproportionation or metal reduction.

This assumption is not fully accurate for all electrochemical systems[37,38], as it neglects possible nonadiabatic effects, but approximates to a reasonable extent the overall energetics of an out-of-equilibrium polarized electrode with flowing current. In this respect in all Li- Na- and K-O_2 batteries the application of small or moderate overpotentials can easily initiate degradation paths originated from the reduction of metal ions to isolated metal atoms. In particular the $O_2^- + LiO_2 \rightarrow {}^3O_2 + Li^0(O_2^-)$ reaction is possibly activated during the discharge of a Li-O_2 battery by the application of an overpotential >0.4 V in respect to the $E°(O_2/LiO_2)$ redox potential. The same reaction channels require overpotentials as small as >0.1 and >0.2 V, in respect to the $E°(O_2/NaO_2)$ and $E°(O_2/KO_2)$ redox potential, respectively, in the case of Na-O_2 and K-O_2 batteries. Such small overpotentials are unavoidable to operate aprotic alkaline-metal-oxygen batteries and are commonly reported in the experimental literature[13,16,17,22,25,43–45]. On the contrary, the release of singlet oxygen requires larger overpotentials (i.e., >0.7, >1.1, >1.2 V for Li, Na, and K, respectively in respect to the corresponding $E°_{O2/MeO2}$)[13,16,17,22,25,43–45].

These thermodynamic data suggest that, during the discharge of aprotic metal air batteries, $^1O_2$ is unlikely to form, unless specific conditions are met. In particular, the adoption of cathodic potential cut-offs below 2.3 V vs Li in the case of Li-O_2 cells, the presence of proton contaminations or weak Lewis acids can initiate $^1O_2$ release, as demonstrated by us in refs. [23,24,46]. The thermodynamic data also indicate that degradation reactions initiated by dimerization of superoxides species and their evolution to the metal reduction channel are energetically accessible under moderate overpotential regimes in the discharge of all aprotic Li-, Na-, K-O_2 batteries. This reaction channel could be responsible for the release of ODR in the discharge of metal-air cells, thanks to its most favorable thermodynamics compared to the singlet oxygen release.

A direct experimental evidence is mandatory to prove the occurrence of this unexpected reaction channel: this goal is beyond the scope of this work, but some comments are appropriate. A possible validation protocol can exploit operando or ex situ nuclear magnetic resonance spectroscopy (NMR) on electrochemical cells or analog chemical environments (e.g., KO_2 disproportion catalyzed by other metals following a strategy adopted by us recently in ref. [46]). NMR has been exploited in battery science in recent years to decipher complex reaction mechanisms for Li and Na electrochemistry as well as O_2 redox reactions in aprotic metal-air cells[47–50]. In particular, the ability of NMR to discriminate magnetic centers in specific bonding environments can be the key to prove the reduction of metal ions to isolated metal atoms during disproportionation reaction in comparison to the expected formation of peroxides.

In Conclusion, we tackled the analysis of the disproportion mechanism of dimeric superoxide species coordinated by sodium, lithium, and potassium ions to mimic the reaction environment of Li-, Na-, and K-O_2 batteries. Our electronic structure calculations and the related thermodynamic evaluations unequivocally show the existence of an additional parasitic redox process besides the expected disproportion to peroxide and molecular oxygen. This additional reaction channel leads to the production of solvated neutral metal atoms. The formation of these species, even in small amounts, might have a negative impact on the performance of aprotic metal-O_2 batteries given their well-known reducing activity and high reactivity towards protic impurities and oxygen molecules.

METHODS

Multireference calculations

All the calculations have been carried out with the ORCA code[51] and with the augmented triple-ζ ma-def2-TZVP[52] basis set. Where possible, the resolution of identity (RI) approximation has also been used. The geometries of the molecules were optimized using the spin-component-scaled version of MP2 perturbation theory (SCS-MP2)[53]. The superoxide complex (the reagent) converges to its triplet ground state, while the singlet triatomic molecule (the product) converges to two different geometries depending on the electronic state. The optimizations, in their restricted variant, converge to the most stable geometry of the peroxide $M^+ \cdots [O_2]^{2-}$ which is a closed shell singlet. When SCS-MP2 is used in its unrestricted broken symmetry formalisms, the optimizations converge instead to the superoxide geometry $M^0 \cdots [O_2]^-$ which is an open shell diradical singlet. The two resulting complexes differ not only by their electronic occupations but also by the [O—O] distance value. Since a diradical singlet is intrinsically non mono-determinantal in character, one should be cautious in using broken symmetry MP2 for its minimum geometry. We have indeed repeated the optimization of one of the trimers using the fully correlated NEVPT2 energies to check the accuracy of the approach. The geometries that we obtained with NEVPT2 and MP2 were essentially identical (see Supplementary Table 1).

To check the convergence of the correlation energy in the chosen basis set, we have repeated one of the calculations using the ma-def2-QZVPP one. The differences in energy were minimal and the relevant data are reported in section Supplementary Methods and in Supplementary Table 2.

In order to properly account for the diradical nature of the species and to determine accurate energies of the electronic states (without relying on inappropriate single-reference ansatz), multi-reference correlated n-electron valence state perturbation theory (NEVPT2)[54,55] has been used at the MP2 geometries. The strongly-contracted NEVPT2 lowest singlet energies were calculated on top of a CASSCF(10,7) wave-function for the MO_2^- triatomics and a CASSCF(18,13) one for the MO_4^- complexes. The active spaces include all the *p* valence electrons and orbitals from the oxygen atoms and the valence *s* orbital of the alkali.

All the NEVPT2 energies were checked against a multi-reference configuration interaction (MRCI) with single and double excitations and Davidson corrections, but the former data have been preferred in this context because of their size consistency.

In order to obtain consistent thermodynamic data, the energy of an isolated $O_2(^3\Sigma)$ or $O_2(^1\Delta)$ molecule at the same computational level was added to the MO_2^- triatomic molecules energies.

Solvent models

These calculations were first performed in vacuum, and then repeated including approximate solvation effects by mean of the implicit solvation model based on solute electron density (SMD) by Cramer and Truhlar[56], using two different parametrized solvents (acetonitrile and diethyl ether). The optimized MP2 geometries were relaxed in the SMD solvents. While it would seem advisable to explore the outcomes of our study using computational setups that include an explicit solvent, we must stress here that this would render the present calculation hardly feasible. CASSCF calculations require a clear-cut configuration space made by a small number of active orbitals. The presence of additional molecules in the

system would inevitably lead to severe performance degradation, more importantly, to active orbital space selection issues and, ultimately to convergence problems.

DATA AVAILABILITY

The data sets generated during and analyzed during the current study are available from the corresponding author on reasonable request.

Received: 12 March 2021; Accepted: 15 July 2021;
Published online: 10 August 2021

REFERENCES

1. Hossain, E., Faruque, H. M. R., Sunny Md, S. H., Mohammad, N. & Nawar, N. A Comprehensive review on energy storage systems: types, comparison, current scenario, applications, barriers, and potential solutions, policies, and future prospects. *Energies* **13**, 3651 (2020).
2. Zeng, Q. et al. Integrated photorechargeable energy storage system: next-generation power source driving the future. *Adv. Energy Mater.* **10**, 1903930 (2020).
3. O'Heir, J. Building better batteries. *Mech. Eng.* **139**, 10–11 (2017).
4. Li, M., Lu, J., Chen, Z. & Amine, K. 30 years of lithium-ion batteries. *Adv. Mater.* **30**, 1800561 (2018).
5. Zhang, H. et al. From solid-solution electrodes and the rocking-chair concept to today's batteries. *Angew. Chem. Int. Ed.* **59**, 534–538 (2020).
6. Bruce, P. G., Freunberger, S., Hardwick, L. J. & Tarascon, J.-M. Li-O2 and Li-S batteries with high energy storage. *Nat. Mater.* **11**, 19–29 (2012).
7. Scrosati, B. Technology: charging towards the superbattery. *Nature* **473**, 448–449 (2011).
8. Choi, J. W. & Aurbach, D. Promise and reality of post-lithium-ion batteries with high energy densities. *Nat. Rev. Mater.* **1**, 1–16 (2016).
9. Tarascon, J. M. Is lithium the new gold? *Nat. Chem.* **2**, 510 (2010).
10. Larcher, D. & Tarascon, J.-M. Towards greener and more sustainable batteries for electrical energy storage. *Nat. Chem.* **7**, 19–29 (2014).
11. Grimaud, A., Hong, W. T., Shao-Horn, Y. & Tarascon, J.-M. Anionic redox processes for electrochemical devices. *Nat. Mater.* **15**, 121–126 (2016).
12. Delmas, C. Sodium and sodium-ion batteries: 50 years of research. *Adv. Energy Mater.* **8**, 17 (2018).
13. Kwak, W. J. et al. Lithium-oxygen batteries and related systems: potential, status, and future. *ACS Appl. Mater. Inter.* **120**, 6626–6683 (2020).
14. Shiga, T., Hase, Y., Kato, Y., Inoue, M. & Takechi, K. A rechargeable non-aqueous Mg-O2 battery. *Chem. Comm.* **49**, 9152–9154 (2013).
15. Reinsberg, P., Bondue, C. J. & Baltruschat, H. Calcium-oxygen batteries as a promising alternative to sodium-oxygen batteries. *J. Phys. Chem. C.* **120**, 22179–22185 (2016).
16. Bi, X., Wang, R., Amine, K. & Lu, J. A critical review on superoxide-based sodium–oxygen batteries. *Small Methods* **3**, 1800247 (2019).
17. Qin, L., Schkeryantz, L., Zheng, J., Xiao, N. & Wu, Y. Superoxide-based K-O2 batteries: highly reversible oxygen redox solves challenges in air electrodes. *J. Am. Chem. Soc.* **142**, 11629–11640 (2020).
18. Aurbach, D., McCloskey, B. D., Nazar, L. F. & Bruce, P. G. Advances in understanding mechanisms underpinning lithium-air batteries. *Nat. Energy* **1**, 1–11 (2016).
19. McCloskey, B. D. et al. Limitations in rechargeability of Li-O_2 batteries and possible origins. *J. Phys. Chem. Lett.* **3**, 3043–3047 (2012).
20. Carboni, M., Marrani, A. G., Spezia, R. & Brutti, S. Degradation of LiTfO / TEGME and LiTfO / DME electrolytes in Li-O 2 batteries. *J. Electrochem. Soc.* **165**, 1–9 (2018).
21. Carboni, M., Marrani, A. G., Spezia, R. & Brutti, S. 1,2-Dimethoxyethane degradation thermodynamics in Li−O 2 redox environments. *Chem. Eur. J.* **22**, 17188–17203 (2016).
22. Qin, B., Chan, K. Y. & Li, C. Y. V. Studies of superoxide degradation kinetics and electrolyte management for a reversible NaO2 battery. *ACS Sustain. Chem. Eng.* **8**, 4317–4324 (2020).
23. Pierini, A., Brutti, S. & Bodo, E. Superoxide anion disproportionation induced by Li^+ and H^+: pathways to 1O2 release in Li−O2 batteries. *ChemPhysChem* **21**, 2060–2067 (2020).
24. Mourad, E. et al. Singlet oxygen from cation driven superoxide disproportionation and consequences for aprotic metal-O2 batteries. *Energy Environ. Sci.* **12**, 2559–2568 (2019).
25. Houchins, G., Pande, V. & Viswanathan, V. Mechanism for singlet oxygen production in Li-ion and metal-air batteries. *ACS Energy Lett.* **5**, 1893–1899 (2020).
26. Mahne, N., Renfrew, S. E., McCloskey, B. D. & Freunberger, S. A. Electrochemical oxidation of lithium carbonate generates singlet oxygen. *Angew. Chem. Int. Ed.* **57**, 5529–5533 (2018).
27. Samojlov, A., Schuster, D., Kahr, J. & Freunberger, S. A. Surface and catalyst driven singlet oxygen formation in Li-O2 cells. *Electrochim. Acta* **362**, 137175 (2020).
28. Wandt, J., Jakes, P., Granwehr, J., Gasteiger, H. A. & Eichel, R.-A. Singlet oxygen formation during the charging process of an aprotic lithium-oxygen battery. *Angew. Chem.* **128**, 7006–7009 (2016).
29. Mahne, N. et al. Mechanism and performance of lithium-oxygen batteries – a perspective. *Chem. Sci.* **8**, 6716–6729 (2017).
30. Mahne, N. et al. Singlet oxygen generation as a major cause for parasitic reactions during cycling of aprotic lithium–oxygen batteries. *Nat. Energy* **2**, 17036 (2017).
31. Aubry, J. M., Rigaudy, J., Ferradini, C. & Pucheault, J. A search for singlet oxygen in the disproportionation of superoxide anion. *J. Am. Chem. Soc.* **103**, 4965–4966 (1981).
32. Nanni, E. J., Birge, R. R., Hubbard, L. M., Morrison, M. M. & Sawyer, D. T. Oxidation and dismutation of superoxide ion solutions to molecular oxygen. Singlet vs. triplet state. *Inorg. Chem.* **20**, 737–741 (1981).
33. Hong, M. & Byon, H. R. Singlet oxygen in lithium−oxygen batteries. *Batteries Supercaps* **4**, 286–293 (2021).
34. Bryantsev, V. S. et al. Predicting solvent stability in aprotic electrolyte Li–Air batteries: nucleophilic substitution by the superoxide anion radical ($O_2^{\bullet-}$). *J. Phys. Chem. A* **115**, 12399–12409 (2011).
35. Marcus, R. A. Electron transfer at electrodes and in solution: comparison of theory and experiment. *Electrochim. Acta* **13**, 995–1004 (1968).
36. Walsh, F. C. Kinetics of electrode reactions: part I - general considerations and electron transfer control. *Trans. Inst. Met. Finish.* **70**, 50–54 (1992).
37. Marcus, R. A. Symmetry or asymmetry of kET and iSTM vs. potential curves. *J. Chem. Soc. Faraday Trans.* **92**, 3905–3908 (1996).
38. Gosavi, S. & Marcus, R. A. Nonadiabatic electron transfer at metal surfaces. *J. Phys. Chem. B* **104**, 2067–2072 (2000).
39. Marcus, R. A. Electron transfer theory and its inception. *Phys. Chem. Chem. Phys.* **14**, 13729–13730 (2012).
40. Marcus, R. A. Electron transfer reactions in chemistry. *Theory Exp. Rev. Mod. Phys.* **65**, 599–610 (1993).
41. Marcus, R. A. On the theory of oxidation-reduction reactions involving electron transfer. I. *J. Chem. Phys.* **24**, 966–978 (1956).
42. Marcus, R. A. & Sutin, N. Electron transfers in chemistry and biology. *BBA* **811**, 265–322 (1985).
43. Elia, G. A. & Hassoun, J. A polymer lithium-oxygen battery. *Sci. Rep.* **5**, 12307 (2015).
44. Park, J., Hwang, J. Y. & Kwak, W. J. Potassium-oxygen batteries: significance, challenges, and prospects. *J. Phys. Chem. Lett.* **11**, 7849–7856 (2020).
45. Sharon, D. et al. Aprotic metal-oxygen batteries: recent findings and insights. *J. Solid State Electrochem* **21**, 1861–1878 (2017).
46. Petit, Y. K. et al. Mechanism of mediated alkali peroxide oxidation and triplet versus singlet oxygen formation. *Nat. Chem.* **13**, 465–471 (2021).
47. Au, H. et al. A revised mechanistic model for sodium insertion in hard carbons. *Energy Environ. Sci.* **13**, 3469–3479 (2020).
48. Yu, S., Liu, Z., Tempel, H., Kungl, H. & Eichel, R. A. Self-standing NASICON-type electrodes with high mass loading for fast-cycling all-phosphate sodium-ion batteries. *J. Mater. Chem. A* **6**, 18304–18317 (2018).
49. Märker, K., Xu, C. & Grey, C. P. Operando NMR of NMC811/graphite lithium-ion batteries: structure, dynamics, and lithium metal deposition. *J. Am. Chem. Soc.* **142**, 17447–17456 (2020).
50. Gauthier, M., Nguyen, M. H., Blondeau, L., Foy, E. & Wong, A. Operando NMR characterization of a metal-air battery using a double-compartment cell design. *Solid State Nucl. Magn. Reson.* **113**, 101731 (2021).
51. Neese, F. Software update: the ORCA program system, version 4.0. *WIREs Comp. Mol. Sci.* **8**, 1327 (2018).
52. Zheng, J., Xu, X. & Truhlar, D. G. Minimally augmented Karlsruhe basis sets. *Theor. Chem. Acc.* **128**, 295–305 (2011).
53. Grimme, S. Improved second-order Møller-Plesset perturbation theory by separate scaling of parallel- and antiparallel-spin pair correlation energies. *J. Chem. Phys.* **118**, 9095–9102 (2003).
54. Angeli, C., Cimiraglia, R., Evangelisti, S., Leininger, T. & Malrieu, J. P. Introduction of n-electron valence states for multireference perturbation theory. *J. Chem. Phys.* **114**, 10252 (2001).
55. Angeli, C., Cimiraglia, R. & Malrieu, J. P. n-electron valence state perturbation theory: a spinless formulation and an efficient implementation of the strongly contracted and of the partially contracted variants. *J. Chem. Phys.* **117**, 9138–9153 (2002).
56. Marenich, A. V., Cramer, C. J. & Truhlar, D. G. Universal solvation model based on solute electron density and on a continuum model of the solvent defined by the

bulk dielectric constant and atomic surface tensions. *J. Phys. Chem. B* **113**, 6378–6396 (2009).
57. Karton, A., Tarnopolsky, A., Lamère, J. F., Schatz, G. C. & Martin, J. M. L. Highly accurate first-principles benchmark data sets for the parametrization and validation of density functional and other approximate methods. Derivation of a robust, generally applicable, double-hybrid functional for thermochemistry and thermochemical kinetics. *J. Phys. Chem. A* **112**, 12868–12886 (2008).

ACKNOWLEDGEMENTS

S.B. would like to thank the University of Rome La Sapienza for the financial support under the grant numbers RM11916B8879F09D and RM120172A46A7608. E.B. and A. P. gratefully acknowledge the University of Rome La Sapienza for support through grants RG120172B4099747 and RM11916B658EF0BA. All authors gratefully acknowledge the computational support of CINECA (grants IsC78_LLL-2 and IsC69_LLL).

AUTHOR CONTRIBUTIONS

A.P. did ab initio calculations and analysed all the results. E.B. conceived and directed the research and S.B. wrote the manuscript. All authors contributed to the discussion and interpretation of the results.

COMPETING INTERESTS

The authors declare no competing interests.

ADDITIONAL INFORMATION

Supplementary information The online version contains supplementary material available at https://doi.org/10.1038/s41524-021-00597-3.

Correspondence and requests for materials should be addressed to E.B.

Reprints and permission information is available at http://www.nature.com/reprints

Publisher's note Springer Nature remains neutral with regard to jurisdictional claims in published maps and institutional affiliations.